REPORT DOCUMENTATION PAGE

Form Approved
OMB No. 0704-0188

1. REPORT DATE *(DD-MM-YYYY)*	**2. REPORT TYPE**	**3. DATES COVERED** *(From - To)*
13-07-2009	Technical Paper	

4. TITLE AND SUBTITLE

On the Effect of a Transverse Acoustic Field on a Flush Shear Coaxial Injector

5a. CONTRACT NUMBER

5b. GRANT NUMBER

5c. PROGRAM ELEMENT NUMBER

6. AUTHOR(S)
Jeffrey Graham, Ivett A. Leyva, & Douglas Talley (AFRL/RZSA); Juan I. Rodriguez (UCLA)

5d. PROJECT NUMBER

5f. WORK UNIT NUMBER
23080533

7. PERFORMING ORGANIZATION NAME(S) AND ADDRESS(ES)

Air Force Research Laboratory (AFMC)
AFRL/RZSA
10 E. Saturn Blvd.
Edwards AFB CA 93524-7680

8. PERFORMING ORGANIZATION REPORT NUMBER

AFRL-RZ-ED-TP-2009-275

9. SPONSORING / MONITORING AGENCY NAME(S) AND ADDRESS(ES)

Air Force Research Laboratory (AFMC)
AFRL/RZS
5 Pollux Drive
Edwards AFB CA 93524-7048

10. SPONSOR/MONITOR'S ACRONYM(S)

11. SPONSOR/MONITOR'S NUMBER(S)
AFRL-RZ-ED-TP-2009-275

12. DISTRIBUTION / AVAILABILITY STATEMENT

Approved for public release; distribution unlimited (PA #09318).

13. SUPPLEMENTARY NOTES
For presentation at the 45th AIAA Joint Propulsion Conference & Exhibit, Denver, CO, 2-5 August 2009.

14. ABSTRACT

An experimental study on the effects of an externally-imposed transverse acoustic field in a flush shear coaxial jet is presented. In this case the inner jet recess is zero and both the inner and outer jet exit planes coincide. Since recess is a design variable used when designing new injectors, this study complements previous studies from this group where the injector geometries included a recess. The shear coaxial injector used here is similar to those used in cryogenic liquid rockets. By using N2 as the working fluid, the chemistry effects are separated from the effects of a transverse acoustic field on coaxial jets. The acoustic field is generated by two piezo-sirens whose resonant frequency is ~3kHz. The acoustic pressures generated are about 2-4% the value of the chamber pressure. The phase angle between these two sources is varied at 45 degree intervals. Two values of pressures are studied, 1.5 MPa (Pr=0.45) where the flow is subcritical and 3.6 MPa (Pr=1.05) where the pressure is nearcritical. The outer to inner jet velocity ratio varies from ~1.5 to 17 and the outer to inner jet momentum flux ratio (J) varies from ~0.09 to 20. These ratios are mainly varied by changing the temperature and flow rates of the outer jet. At least 3000 backlit images were taken at 20-25 kHz for each run. These images are the main analysis tool to study the jet behavior. The most dramatic effects resulting in about 90% reduction of the length of the inner jet core were obtained at nearcritical conditions for the cases of J=1.7 and 3.5.

15. SUBJECT TERMS

16. SECURITY CLASSIFICATION OF:			**17. LIMITATION OF ABSTRACT**	**18. NUMBER OF PAGES**	**19a. NAME OF RESPONSIBLE PERSON**
					Dr. Douglas Talley
a. REPORT	**b. ABSTRACT**	**c. THIS PAGE**	SAR	15	**19b. TELEPHONE NUMBER** *(include area code)*
Unclassified	**Unclassified**	**Unclassified**			N/A

On the Effect of a Transverse Acoustic Field on a Flush Shear Coaxial Injector

Jeffrey J. Graham[1], Ivett A. Leyva[2], Juan I. Rodriguez[3], Douglas Talley[4]
Air Force Research Laboratory, Edwards AFB, CA 93524

An experimental study on the effects of an externally-imposed transverse acoustic field in a flush shear coaxial jet is presented. In this case the inner jet recess is zero and both the inner and outer jet exit planes coincide. Since recess is a design variable used when designing new injectors, this study complements previous studies from this group where the injector geometries included a recess. The shear coaxial injector used here is similar to those used in cryogenic liquid rockets. By using N2 as the working fluid, the chemistry effects are separated from the effects of a transverse acoustic field on coaxial jets. The acoustic field is generated by two piezo-sirens whose resonant frequency is ~3kHz. The acoustic pressures generated are about 2-4% the value of the chamber pressure. The phase angle between these two sources is varied at 45 degree intervals. Two values of pressures are studied, 1.5 MPa (Pr=0.45) where the flow is subcritical and 3.6 MPa (Pr=1.05) where the pressure is nearcritical. The outer to inner jet velocity ratio varies from ~1.5 to 17 and the outer to inner jet momentum flux ratio (J) varies from ~0.09 to 20. These ratios are mainly varied by changing the temperature and flow rates of the outer jet. At least 3000 backlit images were taken at 20-25 kHz for each run. These images are the main analysis tool to study the jet behavior. The most dramatic effects resulting in about 90% reduction of the length of the inner jet core were obtained at nearcritical conditions for the cases of J=1.7 and 3.5.

I. Introduction

OWING to its ubiquity in modern rocket engine design, the sheer coaxial injector has been subjected to intense scrutiny. Its use in the Ariane V rocket Vulcain engine, Atlas V rocket RS-68 engine, and Space Shuttle Main Engine has given it prominence in the field of rocket injectors, making it a strong candidate for use in the next generation of lift vehicles. It is precisely this potential for use in safer, more efficient, and less expensive launch systems that has made a well-grounded understanding of its operational parameters a necessity to avoid unstable combustion.

In this paper, we are concerned primarily with the position of the inner jet post with respect to the exit plane of the outer jet. For cryogenic rocket engines, LOX is usually injected in the center post and hydrogen is injected into the outer jet. Kendrick *et al* [1] observed that a recessed internal LOX post contributed to an increased rate of mixing, and consequently a more rapid flame expansion. They proposed a simple model which indicates that, in a hotfire experiment, a small amount of combustion takes place within the injector recess, which can lead to more efficient mixing by effectively increasing the momentum flux ratio $J = \frac{\rho_g {v_g}^2}{\rho_l {v_l}^2}$ between the outer (gas) and the inner jets (liquid). This is in part corroborated by results from Sasaki *et al* [2] who noticed that by increasing the velocity ratio in a non-recessed swirl injector they could effect an increase in combustion efficiency. Their best performance was with a recessed swirl coaxial injector. Subsequently, Juniper and Candel [3] showed that a recessed inner post has a large region of absolute instability as compared to a flush injector, following from self-sustained wake-like flow instabilities that are seen only intermittently in the flush case. This has been corroborated by the work of Lux and Haidn [4], who found that a recessed LOX post leads to more rapid flame expansion and lesser combustion roughness, both of which are indicative of consistent better mixing. More recently, Moser and

[1] 1st Lt, AFRL/RZSA, Edwards AFB, CA 93524
[2] Post Doctoral Researcher, UCLA/AFRL, Edwards AFB, CA 93524
[3] Lead, Combustion Group, AFRL/RZSA, Edwards AFB, CA 93524
[4]Senior Scientist, AFRL/RZSA, Edwards, AFB, CA 93524

Saffell [5] have noted that increasing the depth of recess improves engine efficiency by less than one percent for one diameter of recess, and slightly over four percent for two injector diameters of recess depth, indicating that the amount of time afforded to the jets to mix within the duct of the outer jet wall is a significant factor for these jets.

Furthermore, it is well known that the combustion chamber is an acoustically active environment. Glogowski *et al* [6] has indicated that the presence of a recess in a coaxial injector can lead directly to a resonant system, and has suggested that a possible mechanism leading to combustion instability is from acoustics in the chamber coupling in to the fuel and oxidizer supply system. Moreover, by spectral analysis, they showed that the system experienced more or less dramatic pressure fluctuations in the chamber plenum according to frequency. With regards to the Rayleigh Criterion, this demonstrates that the presence of a recessed coaxial injector, though capable of producing smooth combustion can, if improperly tuned, set up combustion instabilities. Smith *et al* [7] have continued this line of work by means of numerical models with discrete periodic forcing, which have been validated by experiment. They have demonstrated that the quality of the resonance experienced in the combustion chamber decreases with increasing Mach number of the flow and that the dominant mode, rather than harmonics, are generally responsible for combustion instabilities. Physically, their forcing is the equivalent of the acoustic modes of the injector itself—being a Helmholtz resonator—and they observe that the most deleterious effect on combustion stability occurs when the two modes couple efficiently.

At the Air Force Research Laboratory (AFRL) non-reactive cryogenic experiments have been performed using a shear coaxial injector, with and without transverse acoustic forcing, first by Davis and Chehroudi [8]. Their data, along with data from other researchers they compiled, showed that the inner jet dark core (related to the intact core or potential core) depends on J with a relation of the form $AJ^{-n} + B$, where n is 0.2 for two phase flows (subcritical pressures) and 0.5 for one phase flows (near and supercritical pressures). Since the dark core is a qualitative indicator of mixing in this case, with better mixing achieved with shorter dark cores, then mixing efficiency increases as the velocity ratio and J values increase. Leyva *et al* [9] continued work in this vein by characterizing the behavior of coaxial jets for a wide range of velocity ranges and J values with high speed backlit images (20-40 frames /s). They found that there is an optimum range of J from about 1 to 5 for which acoustics has a statistically significant decrease on the dark core length of the inner jet for all pressures studied. The range is even larger for subcritical pressures. Both of those studies were completed with a fixed phase angle of the acoustic field with respect to the jet location since only one acoustic source was used and the geometry of the experiment was fixed. Rodriguez *et. al* [10] modified the phase angle of the acoustic excitation at the jet location using twin acoustic sources. Their results have shown that acoustic excitation can result in much more rapid mixing than for a similarly acoustics-off case, and moreover that this occurs primarily for a range of J between one and four. For part of that work the same injector as the one being used here was used except that in that case the inner jet was recessed about one half of the inner jet inner diameter value.

Little work, however, has been done on the effect of recess on the interaction of an externally imposed acoustic oscillation with the flow field of coaxial injectors. This research is necessary, however, because recess is a variable that engine designers use to fabricate new injectors.

II. Experimental Setup

The experimental studies reported in this paper were performed at the Air Force Research Laboratory (AFRL) located at Edwards Air Force Base, CA, in the Cryogenic Supercritical Laboratory, EC-4. An overview of the test section is shown in Figure 1. Gaseous N_2 is used to supply the inner and outer jet flows and to pressurize the chamber. The outer and inner jets are cooled by LN2 in heat exchangers (HE's) immediately preceding entry to the chamber; one HE was used for each jet to allow independent temperature (T) control. This was effected by adjusting the flow rate of liquid nitrogen through the HEs. The mass flow rate through the inner and outer jets was measured with Porter mass flow meters (122 and 123-DKASVDAA) prior to cooling, since it was found that it is much easier to measure the flow rates at ambient rather than at cryogenic temperatures. The chamber pressure is measured with a Stellar 1500 transducer. To keep the amplitude of the acoustic oscillations to a maximum near the jet, an inner chamber was created (Figure 1). This inner chamber has a nominal height of 6.6cm, a width of 7.6cm and a depth of 1.3cm. The dimensions of the injector are given in Figure 2A. For all the cases presented here the inner jet was flush with the outer jet.

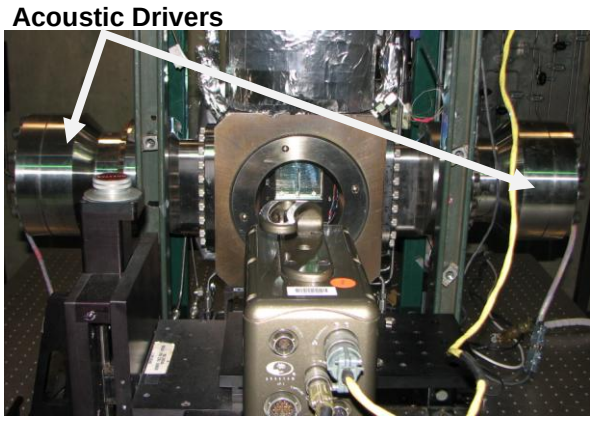

Figure 1. Overview of the Main Chamber of the Supercritical Flow Facility, EC-4 at AFRL/Edwards.

Images of the injector and its placement within the chamber are shown in Figures 2-3, respectively. The temperature of the jets is measured with an unshielded type E thermocouple which has a bead diameter of 0.1mm and an accuracy of ±1 K as checked with an RTD. A Kulite XQC-062 pressure transducer is placed next to the thermocouple and used to measure the pressure at a sampling frequency of 20 kHz. Both the pressure transducer and the thermocouple are moved in a volume around the jet with a piezoelectric positioning system built by Attocube Systems which can move in an area 3mm by 6 mm with step sizes in the order of 0.01mm. Vertical motion is achieved with a fine hand-screw. For temperature profile measurements, the average distance from the exit plane is ~0.3 mm, though the system has the ability to insert the thermocouple into the recess of the injector if so desired. Properties such as density, viscosity, and surface tension are computed from the measured flow rates, chamber pressure and jet temperature, using NIST's REFPROP [10]. From this, the velocity ratio (VR) and J for a given condition can be computed.

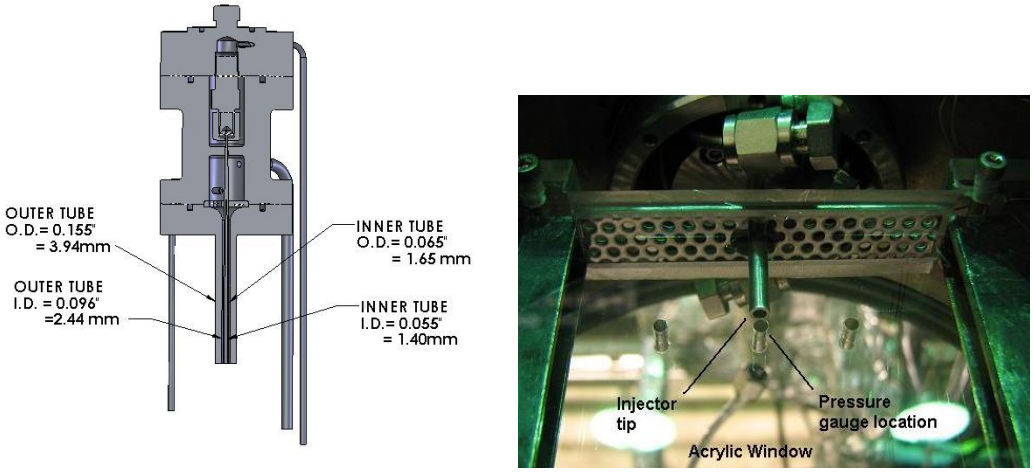

Figure 2. A. Injector Cut-Away. B: Injector Placement

The jet is visualized by taking backlit images using a Phantom 7.1 CMOS camera. The resolution of the images varies from 128x224 to 196x400 depending on chamber pressure and J, which in turn determines the size of the visible features of the jet under scrutiny. Each pixel represents an area of about 0.08 mm x 0.08 mm with a framing rate of 20, 25 or 41 kHz. The jet is backlit using a Newport arc lamp set at 140 W. The acoustic waves are generated using two piezo-sirens custom made for AFRL by Hersh Acoustical Engineering, Inc. (Figure 1). These are operated by providing a sinusoidal signal from a function generator amplified to high voltage for use as the

driving potential. These piezo sirens have a resonant frequency of approximately 3kHz. The specific frequency to use for each run is found empirically by scanning a frequency range from about 2.9 to 3.1 kHz and choosing the frequency that has the most effect on the jet. The distance between the two acoustic sources is about 67 cm and for a nominal driving frequency of 3kHz, there is about 8 wavelengths in this length. However, even the outer diameter of the outer jet is very small compared to the characteristic wavelength so we operate in the long wavelength limit. To accommodate for the rectangular chamber a waveguide with a catenary contour is used to guide the waves from a circular cross-section to a rectangular cross-section (also shown in Figure 1). The sound acoustic pressure in the inner chamber ranges from 7 to 30 kilopascals (1 to 5 psi) peak-to-peak.

III. Experimental Results

A total of 12 conditions were run at subcritical pressure corresponding to a reduced pressure, Pr, of about 0.45, where Pr=Chamber pressure/Critical pressure of N2. For that case, we have two phase flows since the inner jet is at the saturation temperature or a few degrees below and the outer jet is in the vapor phase. A set of 6 conditions were run at nearcritical pressure (Pr=1.05). In this case the jet flow is one phase since both fluids are slightly above the critical pressure. The inner jet temperature is below the critical temperature (liquid-like state) and the outer jet is above the critical temperature. For reference, the critical temperature, Tcr, for N2is 126.3K and the critical pressure, Pcr is 3.4 MPa. For each condition run one or two baseline cases were taken with the acoustics turned off. Then, a series of cases were taken were the phase angle between the two acoustic sources (Figure 1) was varied from 0 to

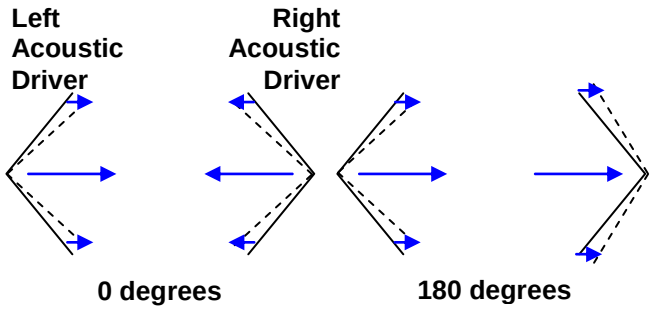

Figure 3. Simplified diagram of the two acoustic drivers at a 0° and 180° phase angle

360 degrees (with 360 being a repeat of 0 degrees) in increments of 45 degrees. This is to capture the full span of acoustic conditions at the jet location, from a pressure antinode to a pressure node. At 0 degrees, the two acoustic sources are in phase and move towards each other as shown in Figure 3. For this case, there is a pressure antinode (velocity node) at the center of the two sources, in other words at the injector location. At 180 degrees, the two sources move away from each other forming a pressure node (velocity antinode) at the injector location.

In what follows some of the most interesting cases run are presented in the form of image collages. For each collage, ten instantaneous back-lit images are shown, each corresponding to a different phase angle tested. The first case to be analyzed is for Pr=0.45 with J=0.09 (Figure 4). This is the limit of a single jet since the outer jet is moving so slowly compared to the inner jet. In the images the inner jet appears darker than the outer jet since it is colder and denser and thus the light from the lamp gets obstructed or deflected the most. For the baseline case, the inner jet does not break within the field of view. Despite the smooth appearance of the inner jet, it is turbulent at Re~104. This case shows a great effect from acoustics. In the phases around 0-45 and 270-360 degrees, the jet is violently destroyed by the acoustics and large sections of the liquid jet, big droplets and ligaments are noticeable after the first break of the jet. In fact, for the case of 45 we can see discrete droplets and their trails. This behavior contrasts sharply with the cases 135, 180, and to some extent 225, where the pressure gradient is small, and the local velocity oscillation is relatively large. In those cases, though the jet moves within the plenum, it moves as a whole, and therefore they have longer dark cores. The 180 degree excitation is particularly interesting in this regard—for some distance down the jet, it looks very nearly like the baseline case. However, necking is observed and

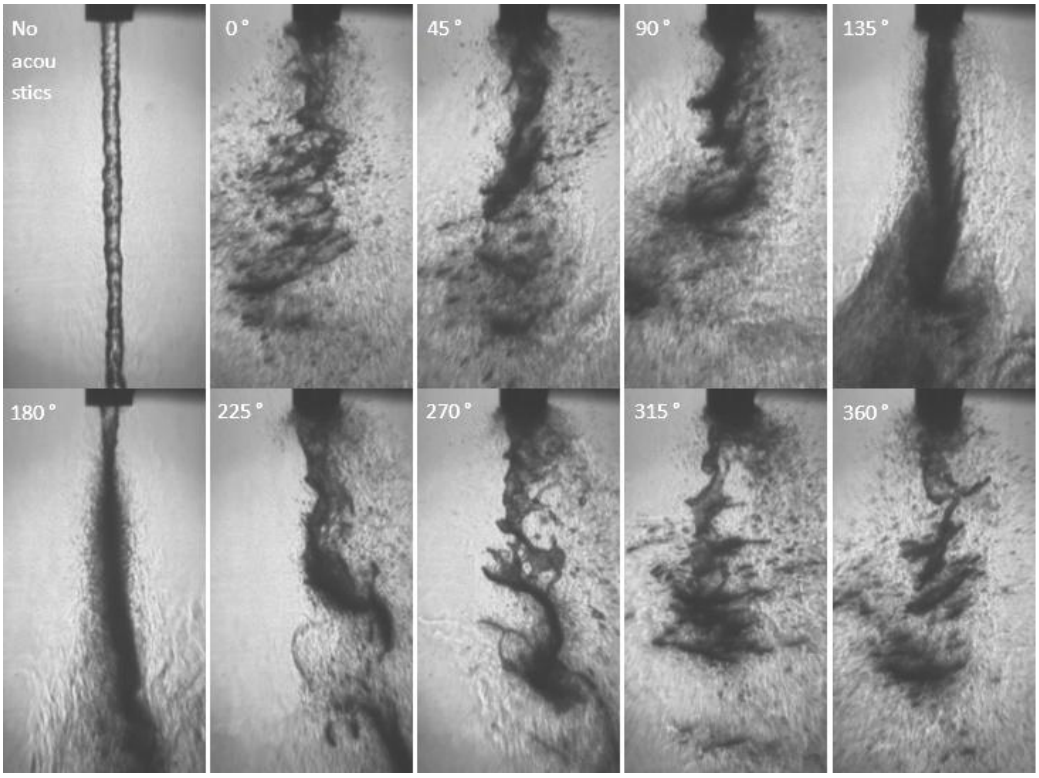

Figure 4. Collection of subcritical coaxial jet images for Pr = 0.45, J = 0.09.

downstream of the neck there is much finer atomization of the jet. Finally note that for all cases except for 180 degrees, there is a toroidal vortex formed at the exit plane of the jet.

The next case is at the same pressure but with J=1.93 (Figure 5). Comparing the baseline with the previous case, one can see that the inner jet is thicker and it breaks down within the field of view. This widening of the inner jet is typical of higher J values. The jet shows more pronounced disturbances in the surface. Also, one can observe a range of droplet sizes as we move downstream from the exit plane. In the baseline case, it is possible to see a glimmer of light through the jet itself, reminiscent of the J=0.09 case. Especially noteworthy is, again, the difference between the 0 and 360 degree cases and those more toward the 180 phase. In all cases except 180 there are clear images of vortices forming on the surface of the inner jet. Since vortex lines can only terminate on walls, they must either penetrate the whole of the outer jet to terminate on the windows, without connecting, or form an annulus around the inner jet. The latter seems rather more likely. The cause for this corresponds to the compression and rarefaction around the inner jet caused by the acoustics. Certainly, the inner jet does break down in a similar fashion to the 0.09 case down the center line, but only after a sufficient length to allow for mixing. One further point is that, as the flow rates for the inner jet in both cases were very close, only the change in the outer jet can account for this particular change in spray behavior. At 45 and 90 degrees there is region downstream from the first vortical structure with very fine droplets. At 180 degrees where we have a pressure node at the jet location there is a lack of toroidal vortex formation. The jet is being moved as a whole. Cases 135 and, to some extent, 225, are particularly notable insofar as they show a transition from one behavior to the other.

.

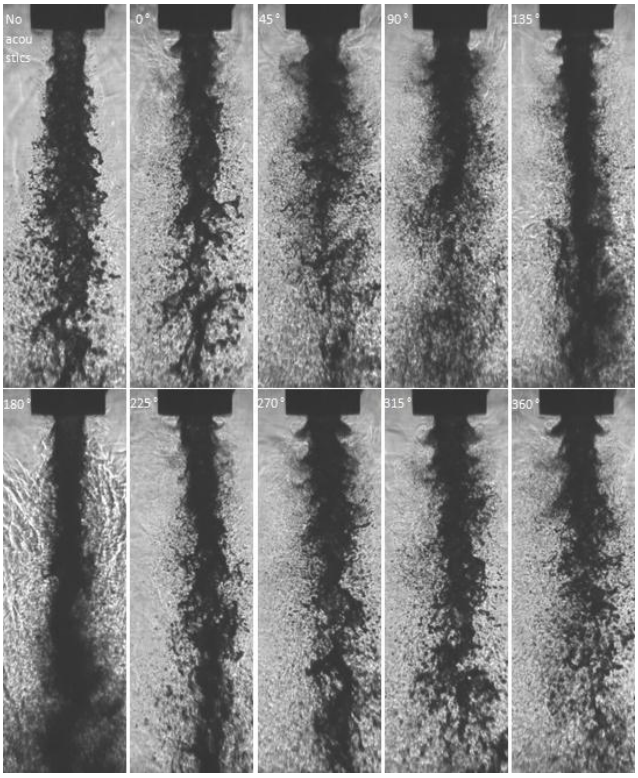

Figure 5. Collection of subcritical coaxial jet images for Pr = 0.45, J = 1.93

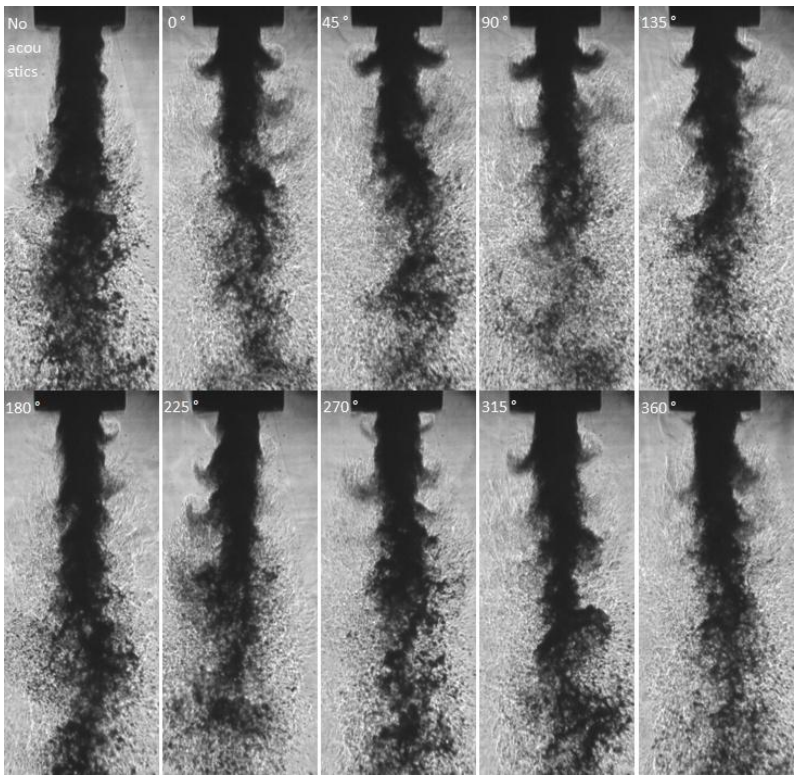

Figure 6. Collection of subcritical coaxial jet images for Pr = 0.45, J = 7.9

For the following case of J=7.9 (Figure 6), changes are occurring more with respect to intensity rather than fundamental form. Whereas the 0.09 case and, to some extent, the 1.93 case showed evidence surface disturbances in the inner jet for the baseline cases, in this case the outer jet has sped up and is carrying considerably more momentum, such that it blows along the surface of the inner jet and generates surface disturbances, much as a wind would do on a lake. Furthermore, the annular vortices of the boundary are significantly more pronounced in the 0 through 90 degree cases—the presence of a strong black protrusion from the center jet indicates that mass jet from the inner is being pulled away quite strongly in these cases. At the other phase angles mass is still being pulled from the inner jet to some extent, but not nearly as much, and the vortex appears to involve mass moslty from the outer boundaries of the inner jet and the outer jet. For the 180° case, as well as the 225° to a lesser extent, the vortices do not form nearly as strongly. There are a few, to be sure, but they lack the symmetry and persistence of the previously discussed cases.

The last case to be analyzed is that of J=18 (Figure 8). Here one can see how the dramatically larger velocity of the outer jet as compared to the inner jet manifests itself. Observe how the vortices which have appeared in prior cases, though still present, appear more thoroughly stretched vertically, and develop further down from the injector exit plane. The outer jet, besides being a key component in the formation of the vortices, is pulling them downstream considerably faster than if they convected downstream at the inner jet velocity. This does not appear to be happening in the 180 case. The baseline case shows the formation of spray generally in the vertical axis, with some, not particularly strong, expansion to the left and the right, while all the acoustically driven cases show stronger fragmentation earlier. One final point: on the 180 degree excitation, there are what appear to be pulses of inner core matter protruding out at regular intervals and at alternating vertical position, serving as a dramatic illustration of the effects that the alternating velocity of the surrounding plenum have on the jet as it emerges in to the chamber, and that it builds to some extent, but appears to either stop growing, or grow slowly enough that it disperses before the effect becomes truly pronounced.

Next we will explore the cases taken at nearcritical pressures (Pr=1.05). The first two cases to be discussed have J=1.7 (Figure 8) and 3.5 (Figure 9). These are very dramatic cases illustrating the effects of both acoustics and phase angle. Owing to their striking similarity, the authors have decided to discuss them simultaneously. Of course, the most noteworthy occurrence in these cases is the total annihilation of the inner jet dark core at phases 90 and below or 270 and above at J=1.7, and a similar, though not as dramatic, behavior in the J=3.5 case. At J=1.7, for phase angles of 90 and 135 degrees, there are two, or three vortical structures that are closely spaced and then collapse in to a well-mixed jet. At J=3.5, there are two or three vortical structures that are much more widely spaced. A natural inference is that the increase in spacing follows from the increased outer jet velocity. The driving frequency for J=1.7 was 3.09kHz, and for J= 3.5 it was 3.06kHz, such that this could not account for this change. The images were taken at a rate of 20kHz, such that the difference in the driving frequencies should not show up in a single frame. Only on the average would it arise, which is not the circumstance under consideration. One could ask why should the jet be so profoundly truncated in these near-critical cases, when the subcritical cases showed no such dramatic shortening. Certainly we still see that the greatest effect is a at the pressure antinode (0 degrees) like in previous cases where the pressure fluctuations are maximum. Close to the pressure node (180, 225 degrees), where the velocity fluctuations are the largest the jet remains the longest, or least affected. Also the vortical structures are not as prominent as for the rest of the cases. Any differences between what is happening now and what happened in the sub-critical case seem to be of magnitude and not of kind.

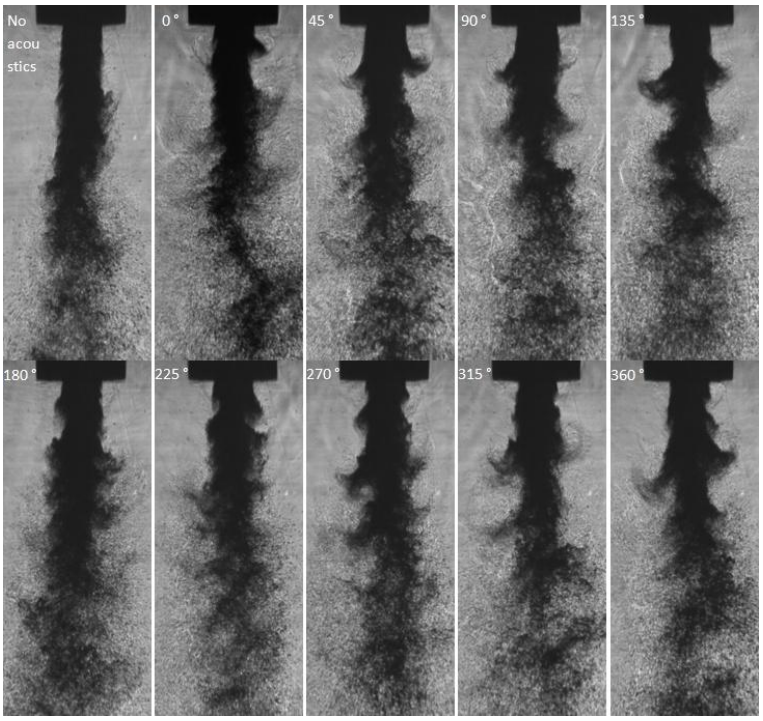

Figure 7. Collection of subcritical coaxial jet images for Pr = 0.45, J = 18

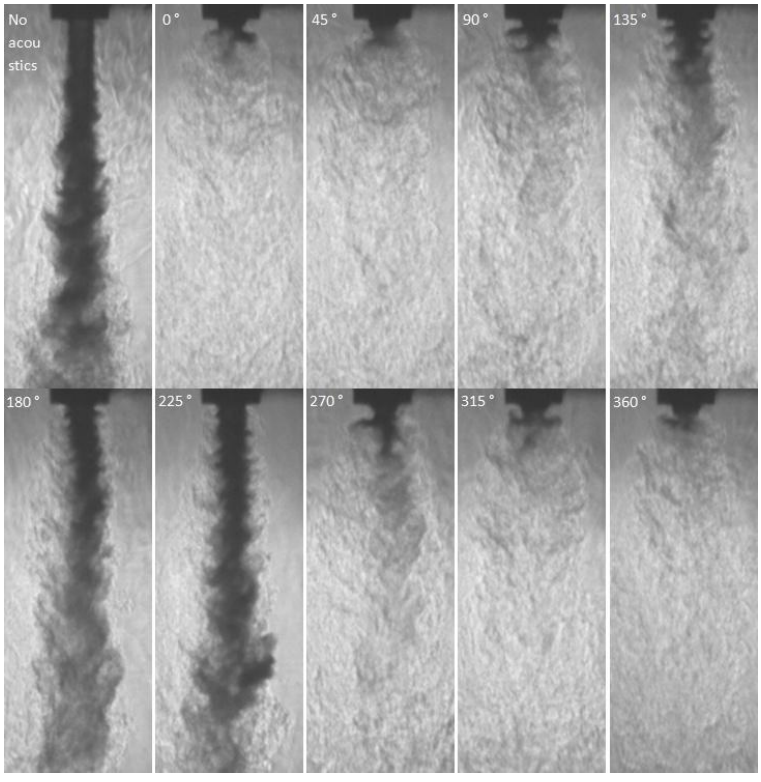

Figure 8. Collection of nearcritical coaxial jet images for Pr = 1.04, J = 1.7

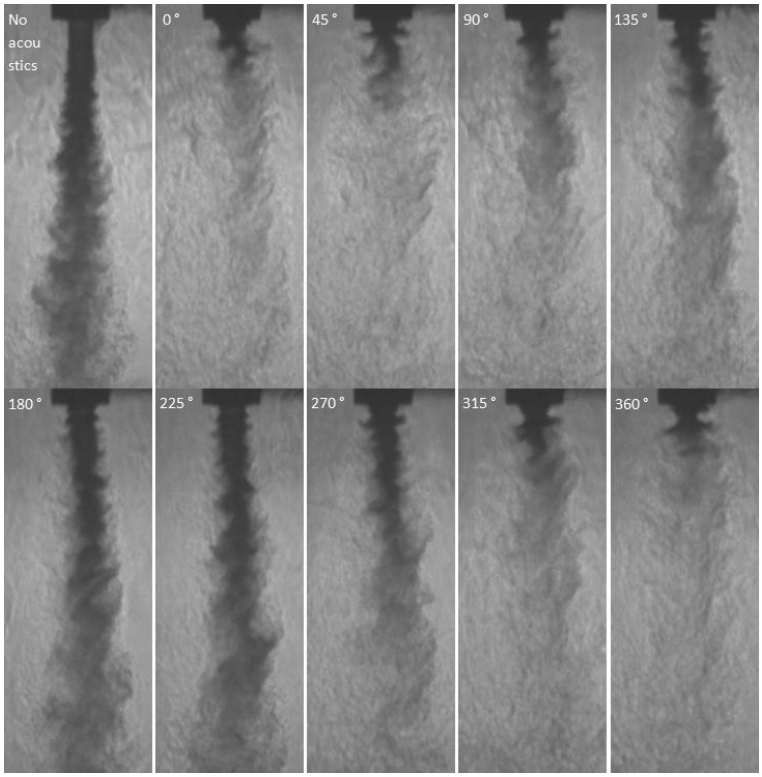

Figure 9. Collection of nearcritical coaxial jet images for Pr = 1.04, J = 3.5

For the case of J=10 (Figure 10), the acoustics are having less of an effect, similar to what the subcritical cases showed at the largest momentum flux ratios. The toroidal vortices are still apparent though. The baseline case is longer than the rest, implying that acoustics do affect mixing, but the effect is not linked to the phase angle. In the baseline case, the primary mixing mechanism between the two jets is the velocity gradient, or shear, between the two jets. The acoustics, however, drive the outer jet in to the inner jet by pressure or velocity gradients, and then strong mixing occurs for certain conditions. The large vortical structures prompted by the acoustics act as mixing enhancements for the jet. The last case corresponds to J=20 (Figure 11). This case corroborates the points made in the J=10 case. The inner jet dark core for the baseline is significantly longer than the perturbed cases; but the dark cores for the perturbed cases are about equal regardless of the phase angle. Therefore, once perturbed, the system collapses into one basic mixing regime, regardless of the phase of the perturbation. Since they are shorter than the J=10, their mixing is more rapid, and the chief difference between the two is the momentum flux of the outer jet. Consequently, in this high J condition, all the perturbations introduced collapse the system and it assumes a mixing length based primarily on J.

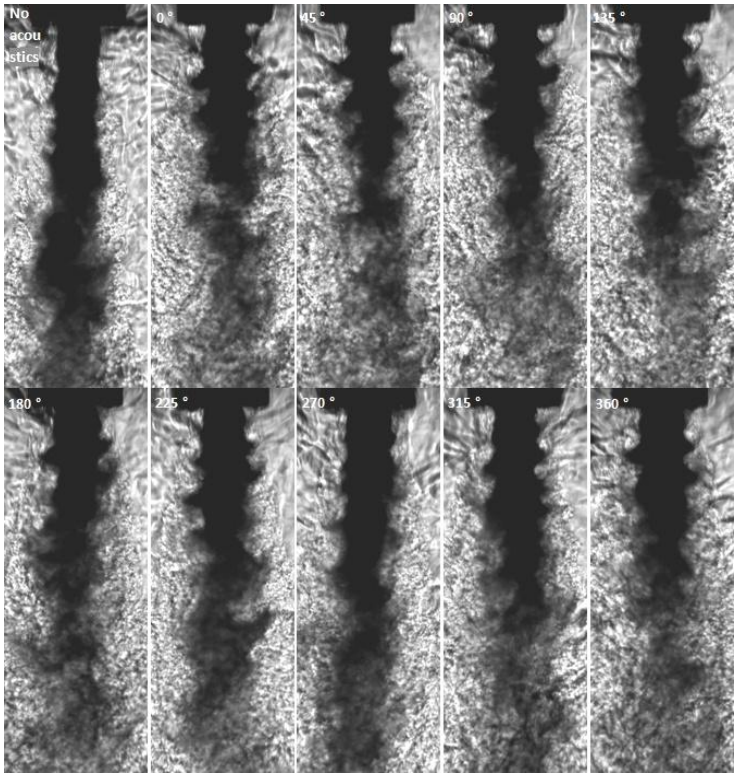

Figure 10. Collection of subcritical coaxial jet images for Pr = 1.04, J = 10

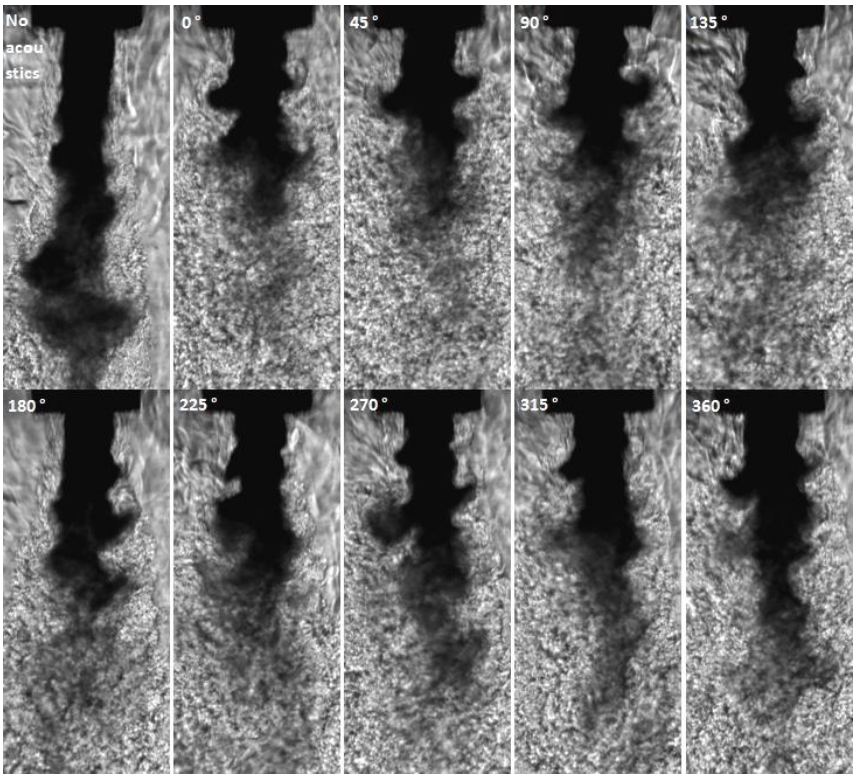

Figure 11. Collection of subcritical coaxial jet images for Pr = 1.04, J = 20.

Finally, we can put all these results together in the form of plots of the dark core length at the various phase angles normalized by the dark core length at the baseline case. Figure 12 shows the results for the case of subcritical pressure. In here we can see that for the two lower J values, 0.09 and 0.36, the largest reduction is for a pressure antinode and the jet is less reduced close to the pressure node. The case for J=1.93 is very interesting since it would seem like the jet is actually getting longer at the pressure node. This should be taken with a word of caution. The way the dark core length is calculated is solely based on thresholding the image to black and white pixels depending on the distribution of the brightness of the image. That is, the routine cannot distinguish very well between a continuous dark core and an agglomeration of very fine droplets, which is more like what is happening here. The point to take away is that for the case J=1.93 there is very fine atomization occurring close to the pressure node, which makes the dark core appear longer. As the J value increases the reduction decreases and the dependence with phase angle also ceases. For the case of Nearcritical pressures (Figure 13), the results are qualitatively the same, except that we don't have a case with J=1.93 so we can't make a direct comparison with the similar case in the subcritical regime. Also note that for J=1.6 and 3.47 there are dramatic reductions on the dark core length at the pressure antinode. Finally for the case of J=20 there does not seem to be a dependence on the phase angle.

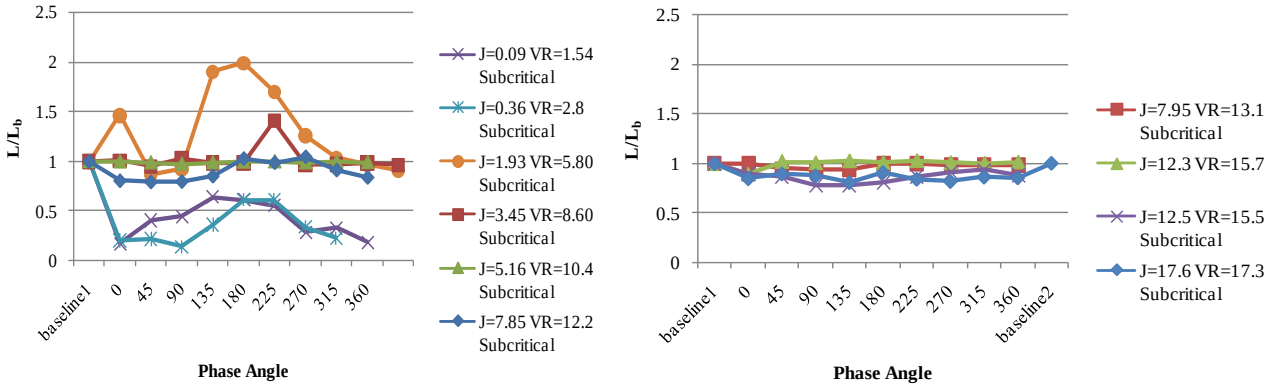

Figure 12. Normalized Inner Jet Dark Core Length as a Function of Phase Angle for Subcritical Pressure.

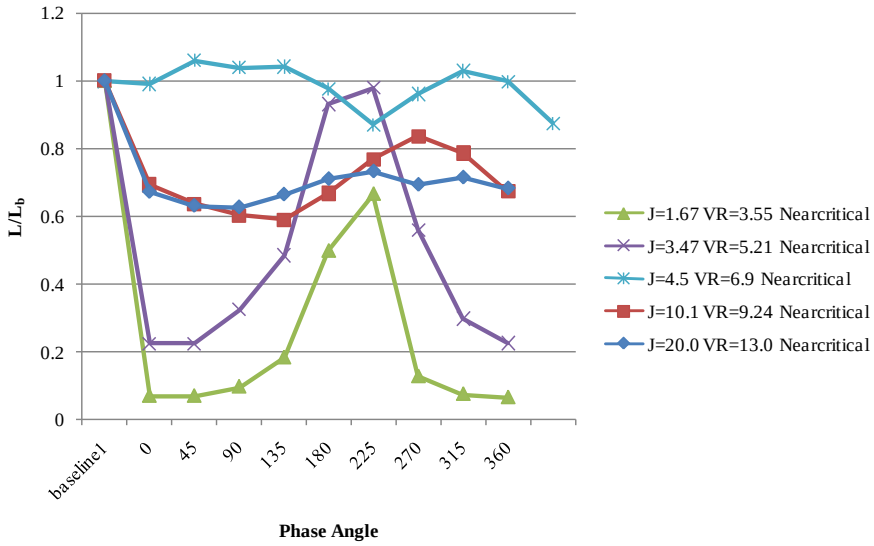

Figure 13. Normalized Inner Jet Dark Core Length as a Function of Phase Angle for Nearcritical Pressure.

IV. Conclusions

An experimental study was carried out to explore the effects of a transverse acoustic field on a flush shear coaxial injector. The magnitude of the acoustic pressure was 1.7-4% the mean chamber pressure. Two chamber pressures were studied, 1.5 MPa (Pr=0.45) and 3.5 MPa (Pr=1.05). The outer to inner jet velocity ratio varies from ~1.5 to 17 and the outer to inner jet momentum flux ratio (J) varies from ~0.09 to 20. It was found that for the single jet limit in the case of the subcritical pressures the jet was destroyed by the acoustics close to a pressure antinode. At the other extreme, the pressure node, the jet exhibited necking and fine vaporization downstream of the neck. For moderate ranges of J values (1.9-7.8) the jet responded to the phase of the acoustic field with the largest reduction around the pressure antinode. Large vortical structures emanating from the inner jet and enhancing the mixing between the two jets were evident for these cases, except for the case of pressure nodes, where such structures were much less conspicuous. The shedding frequency of the vortical structures coincides with the driving frequency. For the case of J=18, the effect of acoustics became independent of phase angle. While there was still a reduction on the core length, it was about the same for all cases. The vortical structures were still evident for this case but less pronounced than in lower J cases.

The most dramatic effects were found for the nearcritical pressure for J=1.7 and 3.5. For those cases, the reduction of the dark core at the pressure antinode was about 90% of the baseline case. For those cases, you can still see vortical structures but they involve the whole inner jet flow and downstream of the first one or two vortical structures, one cannot distinguish the inner jet anymore. Complete mixing seems to have been achieved. As the J number increased, the effect diminished quantitatively but remained the same qualitatively. Except for the case of J=20 where the reduction in dark core also became independent of phase angle.

Acknowledgements

The authors would like to express their appreciation to Mr. Randy Harvey for his invaluable contributions in running and maintaining the facility. This work is sponsored by AFOSR under Mitat Birkan, program manager.

Appendix

Table 1. Run Conditions

	$T_{chamber}$ (K)	$\rho_{chamber}$ (kg/m^3)	$P_{chamber}$ (MPa)	T_{outer} (K)	$\dot{m}_{outer}$ (mg/s)	ρ_{outer} (kg/m^3)	u_{outer} (m/s)	T_{inner} (K)	$\dot{m}_{inner}$ (mg/s)	ρ_{inner} (kg/m^3)	u_{inner} (m/s)	Freq. (kHz)	VR
	Spreading Angles											P'_{RMS} (kPa)	J
	Baseline	φ=0°	φ=45°	φ=90°	φ=135°	φ=180°	φ=225°	φ=270°	φ=315°	φ=360°			
SUB													
sub1	248	20	1.49	207	89.8	25	1.4	101	920	688	0.87	3.04	1.54
Left	0.7	9.8	10.8	7.9	0.0	1.6	2.8	8.6	10.4	2.9			
Right	1.5	0.9	2.0	3.3	0.2	0.0	0.2	11.1	13.4	1.5		5.2	0.09
sub2	208	25	1.50	150	525	37	5.6	106	942	654	0.94	2.96	6.00
Left	5.9	2.2	2.7	2.1	1.0	4.9	1.3	0.5	0.8	1.8	6.59		
Right	6.6	2.7	4.9	4.1	5.1	4.6	0.7	6.4	8.5	6.9	7.24	6.7	1.93
sub3	207	25	1.50	164	999	33	12	112	944	62	9.9	3.04	12.2
Left	7.2	3.0	2.3	4.1	2.5	3.3	4.6	1.5	1.3	1.2	6.75		
Right	5.0	3.4	3.5	3.6	3.4	4.3	3.2	5.2	8.3	3.7	4.29	7.0	7.85
sub4	198	25	1.50	150	1590	37	17	112	944	62	9.9	3.06	17
Left	8.1	5.7	5.0	3.1	3.6	8.9	5.8	5.1	3.7	3.5	6.7		
Right	4.4	4.7	4.1	5.1	2.6	3.4	4.2	5.8	5.4	5.5	4.41	5.6	17
NEAR													
near1	216	59	3.57	176	730	78	3.7	120	938	556	1.1	3.09	3.5
Left	4.5	-10.125	-12.095	10.13	3.9443	1.4675	2.86	4.5739	-0.9548	-15.945			
Right	3.9	-14.036	-4.0856	-3.271	7.7935	4.2518	3.53	3.0612	0.9548	8.1301		9.0	1.7
near2	210	61	3.57	186	1035	72	5.7	122	936	530	1.2	3.06	5.2
Left	6.5	-0.6031	-3.0128	1.22	2.473	1.608	0.8732	3.3122	0.3465	0.2154			
Right	3.9	-3.3564	-3.2705	4.867	9.3488	7.0152	6.1545	7.4685	3.4382	-1.6796		7.6	3.5
near3	255	48	3.57	172	1714	81	8.4	112	942	629	0.98	2.98	9.2
Left	8.3	2.4842	3.4215	2.931	3.2538	2.5712	1.4229	8.0216	1.7574	4.1504	11.2		
Right	4.3	6.2548	5.4064	5.477	5.1678	2.9249	5.35	2.5035	3.579	8.2739	5.54	5.9	10
near4	202	64	3.57	183	2407	73	13	112	945	629	0.98	3.05	13
Left	8.759	4.6884	4.8396	3.571	6.0411	5.7863	4.4842	5.814	6.112	5.5606	11.4		
Right	2.2434	3.5101	3.6873	3.901	4.0097	3.4542	4.4122	4.8055	5.2066	5.3308	11.4	6.1	20

References

[1] Kendrick, D., Herding, G., Scouflaire, P., Rolon, C., and Candel, S., Effects of a recess on cryogenic flame stabilization. Combustion and Flame 118:327-339 (1999)

[2] Sasaki, M., Sakamoto, H., Takahashi, M., Tomita, T., Tamura, H., "Comparative study of recessed and non-recessed swirl coaxial injectors," AIAA-1997-2907-657, 1997.

[3] Juniper, MP., and Candel, SM. "The stability of ducted compound flows and the consequences for the geometry of coaxial injectors," *Journal of Fluid Mechanics* (2003), vol 482, 257-269.

[4] Lux, J. and Haidn, O. Effect of Recess in High-Pressure Liquid Oxygen/Methane Coaxial Injection and Combustion. Journal of Propulsion and Power, Vol. 25, No. 1, Jan-Feb 2009.

[5] Moser, M.D. and Saffell, R.J., GOX/Methane Injector Effects on Combustion Efficiency. AIAA 2008-4952

[6] Glogowski, M. et al. Shear Coaxial Injector Stability Mechanisms. AIAA-1994-2774

[7] Smith, R. et al. Computational Investigation of acoustics and instabilities in a longitudinal-mode rocket combustor. AIAA Journal Vol 46, no. 11, Nov 2008, AIAA-28125-723.

[8] Davis, D. W., Chehroudi, B., Sorensen, I., "Measurements in an Acoustically Driven Coaxial Jet Under Supercritical Conditions," AIAA-2005-736, 2005.

[9] Leyva, I. A., Rodriguez, J.I., Chehroudi, B., Talley, D., "Preliminary Results On The Effect Of Phase Angle On Coaxial Jet Behavior Spanning Sub- To Supercritical Pressures," ILASS 08-A142, 2008.

[10] Leyva, I. A., Rodriguez, J.I., Chehroudi, B., Talley, D., "Preliminary Results on Coaxial Jet Spread Angles and the Effects of Variable Phase Transverse Acoustic Fields," AIAA-2008-950, 2008.

[11] REFPROP, Reference Fluid Thermodynamic and Transport Properties, Software Package, Ver. 7.0, NIST, U.S. Department of Commerce, Gaithersburg, MD, 2002.

[12] Branam, Richard and Mayer, Wolfgang, "Characterization of Cryogenic Injection at Supercritical Pressure," JPP, Vol 19, No 3, 2003.